



doi: 10.1111/pce.12348

Original Article

UV-B mediated metabolic rearrangements in poplar revealed by non-targeted metabolomics

Moritz Kaling^{1,2}, Basem Kanawati², Andrea Ghirardo¹, Andreas Albert¹, Jana Barbro Winkler¹, Werner Heller³, Csengele Barta⁴, Francesco Loreto⁵, Philippe Schmitt-Kopplin² & Jörg-Peter Schnitzler¹

¹Research Unit Environmental Simulation, Institute of Biochemical Plant Pathology, ²Research Unit Analytical BioGeoChemistry and ³Institute of Biochemical Plant Pathology, Helmholtz Zentrum München, D-85764 Neuherberg, Germany, ⁴Department of Biology, Missouri Western State University, St. Joseph, MO 64507, USA and ⁵Department of Biology, Agriculture and Food Sciences, The National Research Council of Italy (CNR-DISBA), 00185 Roma, Italy

ABSTRACT

Plants have to cope with various abiotic stresses including UV-B radiation (280-315 nm). UV-B radiation is perceived by a photoreceptor, triggers morphological responses and primes plant defence mechanisms such as antioxidant levels, photoreapir or accumulation of UV-B screening pigments. As poplar is an important model system for trees, we elucidated the influence of UV-B on overall metabolite patterns in poplar leaves grown under high UV-B radiation. Combining non-targeted metabolomics with gas exchange analysis and confocal microscopy, we aimed understanding how UV-B radiation triggers metabolome-wide changes, affects isoprene emission, photosynthetic performance, epidermal light attenuation and finally how isoprene-free poplars adjust their metabolome under UV-B radiation. Exposure to UV-B radiation caused a comprehensive rearrangement of the leaf metabolome. Several hundreds of metabolites were up- and down-regulated over various pathways. Our analysis, revealed the up-regulation of flavonoids, anthocyanins and polyphenols and the down-regulation of phenolic precursors in the first 36 h of UV-B treatment. We also observed a down-regulation of steroids after 12 h. The accumulation of phenolic compounds leads to a reduced light transmission in UV-B-exposed plants. However, the accumulation of phenolic compounds was reduced in non-isoprene-emitting plants suggesting a metabolic- or signalling-based interaction between isoprenoid and phenolic pathways.

Key-words: Populus × *canescens*; Fourier transform ion cyclotron resonance mass spectrometry.

INTRODUCTION

Plants are sessile organisms and have to cope with various abiotic stresses including ultraviolet radiation (UV, 280–400 nm), in particular high-energy, short-wave length UV-B radiation (280–315 nm), which is one of the components of sunlight. The amount of UV-B radiation that reaches earth's surface depends on latitude, season, time of day, cloud

Correspondence: J.-P. Schnitzler. E-mail: jp.schnitzler@helmholtz -muenchen.de

cover and altitude (Seckmeyer et al. 2008). Hence, the quantity of UV-B radiation that reaches a plant species has significant effects on terrestrial ecosystems (Caldwell et al. 2007). Natural levels of UV-B radiation act as an environmental regulator controlling gene expression, plant growth and development (Jenkins 2009; Hideg et al. 2013). A high UV-B dose negatively affects cellular/subcellular and macromolecular structures in the vegetative plant tissue, including DNA (Britt 1995), RNA and protein damage, reduce photosynthesis, biomass and seed production and modulate the plant's architecture (Strid et al. 1994; Jansen et al. 1998; Ries et al. 2000; Jenkins 2009). It also causes mutations in the germ line manifest in the next generations (Ries et al. 2000). Thus, plants have to sense natural UV-B radiation and quickly respond to high levels of UV-B radiation, making acclimation possible (Jenkins 2009). Recently, the UV-B photoreceptor UV RESISTANCE LOCUS 8 (UVR8) was discovered in Arabidopsis thaliana. This receptor triggers morphology and primes plant defence mechanisms such as antioxidant levels, photoreapir or accumulation of UV-B screening pigments (Rizzini et al. 2011; Heijde & Ulm 2012). Over the last decades, it has been shown that certain plant metabolites, such as flavonoids (Li et al. 1993; Lavola 1998; Kaspar et al. 2010), phenolics (Warren et al. 2003; Kusano et al. 2011; Tossi et al. 2011), ascorbate (Costa et al. 2002; Lidon et al. 2012) and tocopherol (Carletti et al. 2003), actively protect plants against harmful UV-B radiation. These compounds operate either as UV-B absorbing metabolites in the epidermal cell layers attenuating, UV-B transmission into the mesophyll layer, in turn protecting the photosynthetic apparatus (Burchard et al. 2000), or they secure the plant cell against reactive oxygen and reactive nitrogen species (ROS/ RNS) that are produced during the stress response (Lidon et al. 2012; Hideg et al. 2013). Such a function is also attributed to isoprene (2-methyl 1,3-butadiene), a biogenic volatile organic compound (BVOC), which is emitted in significant amounts from many tree species such as poplars and oaks (Loreto & Schnitzler 2010). Isoprene is thought to have an important adaptive function against abiotic stress (Loreto & Schnitzler 2010; Monson et al. 2013) including temperature (Behnke et al. 2007), drought (Sharkey & Loreto 1993; Brüggemann & Schnitzler 2002) and increased UV-B

radiation (Harley et al. 1996; Tiiva et al. 2007). Synthesis of isoprene strongly depends on photosynthetic active radiation (PAR, 400-700 nm) intensity (Hanson & Sharkey 2001). Based on the existing data (Harley et al. 1996; Tiiva et al. 2007), it cannot be unambiguously assigned that UV-B radiation directly or indirectly impairs isoprene emission. Poplar is an excellent tree model to study the biological functions of isoprene (Schnitzler et al. 2010). Transgenic poplar lines almost completely suppressed in isoprene emission (Behnke et al. 2007) allow the study of isoprene functions in an almost identical genetic background compared with the isopreneemitting wild type (WT). It has been observed that under abiotic stress, the absence of isoprene [knocked-down by RNAi (Behnke et al. 2007)] resulted in a new chemotype with suppressed production of phenolic compounds (Behnke et al. 2010).

Fourier transform ion cyclotron resonance mass spectrometry (FT-ICR-MS) provides high resolution and mass accuracy and therefore, is the perfect match for non-targeted metabolomic analysis (Aharoni et al. 2002; Forcisi et al. 2013). Up to now, metabolomics have been scarcely used to analyse overall metabolic changes in plants under or following UV-B stress. The few published studies either use well established A. thaliana mutants, for example, deficient in flavonoid production (tt4 and tt5 mutants; Kusano et al. 2011), impaired in sinapoyl malate production (sinapoyl glucose accumulator 1, sng1; Kusano et al. 2011) or mutants sensitive to UV-B radiation (fah-1; Lake et al. 2009) or they use medicinal plant species like Melissa officinalis (Kim et al. 2012). These few experiments clearly demonstrate that UV-B radiation triggers an overall metabolomics rearrangement of almost all metabolic pathways (Lake et al. 2009; Kusano et al. 2011).

To further answer these questions, we used direct injection (DI) FT-ICR-MS combined with gas exchange analysis as well as confocal laser scanning microscopy (cLSM) to elucidate whether suppression of isoprene by RNAi interferes with wide changes in metabolic profiles and overall physiological behaviour during adaptation of grey poplar [Populus × canescens syn. P. alba × P. tremula (Aiton.) Smith] to UV-B radiation. Therefore, we used non-isoprene-emitting (NE) and isoprene-emitting (IE) poplar lines (Behnke et al. 2007), which first were grown in the absence of UV radiation to a 20-leaf stem stage and then exposed to high UV-B irradiation of 2.8 W m⁻² and 19 W m⁻² of UV-A radiation (315–400 nm) in sun simulators (Thiel et al. 1996) over 13 consecutive days.

We aimed to understand how UV-B radiation (1) triggers overall metabolic changes, (2) affects isoprene emission, photosynthetic performance, epidermal light attenuation and finally (3) how isoprene-free poplars adjust their metabolome under high UV-B radiation.

MATERIAL AND METHODS

Plant material

We used two transgenic non-isoprene-emitting (NE) grey poplar [*Populus* × *canescens* syn. *P. alba* × *P. tremula* (Aiton.)

Smith] lines (Ra2, Rb7), in which the transcription of isoprene synthase (ISPS, EC = 4.2.3.27) is knocked-down by RNA-interference (RNAi). The Ra2 vector construct consists of a gene segment from the transit peptide sequence (Behnke *et al.* 2007), whereas the RNAi vector of Rb7 targets a gene sequence of the core peptide (for detailed information, see Supporting Information). Additionally, two isoprene-emitting (IE) lines, that is, wild type (WT) and empty vector (EV) were used.

Growth conditions

For the experiment, 1-year-old saplings were cut back and put in the greenhouse. From each poplar line, we cultivated eight plants under exclusion of UV-B irradiation. When plants reached the 20-leaf stem stage, they were transferred into the sun simulators of the Research Unit Environmental Simulation at the Helmholtz Center Munich (Neuherberg, Germany; Thiel et al. 1996) for an acclimation phase of 10 d (Supporting Information Fig. S1a,b, day/night = 16/8 h). Temperature profiles were 27/17 °C and relative humidity 40/80%. Daily maximum intensity of PAR for 8 h was slowly increased from 500 to 1400 µmol m⁻² s⁻¹. After acclimation, plants were divided into batches. Half of each group (NE, IE) were transferred into the chambers were UV-B stress was generated (treatment chambers, Supporting Information Fig. S2), by providing a supplementary maximum UV-B irradiation of 2.8 W m⁻² – getting 1.1 W m⁻² biological effective UV-B radiation after (Green et al. 1974) according to measurements of (Caldwell 1971) normalized at 300 nm - and 19 W m⁻² UV-A radiation (315–400 nm) over 13 consecutive days (Supporting Information Fig. S1). The other half was cultivated without UV application but apart from that under identical environmental conditions (control chambers). PAR intensity in both scenarios was at 1400 μ mol m⁻² s⁻¹. All spectral measurements were performed using a double monochromator system TDM300 (Bentham, Reading, England).

The experiment was split into two parts. In the first experiment WT and Ra2 grey poplar plants were exposed to UV-B radiation and EV and Rb7 poplar lines were used for the second experiment. To exclude chamber effects the treatment and control chambers were switched for the second run. To allow the measurements, one chamber was run two hours in delay to the other.

Sampling

Leave samples were taken after plants went through the entire daily length of maximum UV irradiation (16:00–18:00 h; Supporting Information Fig. S1). Throughout the experiment the three leaves above and below leaf 9 were randomly harvested at seven different time points, that is, at days 0, 1, 2, 3, 5, 9 and after finishing measurements at day 13, leaf number 9 was harvested. For sampling, the leaves were immediately thrown into liquid nitrogen. Afterwards, the leaves were grounded in the presence of liquid nitrogen into a fine powder and stored at -80 °C for further analysis.

cLSM

After 13 d of UV exposure, leaf number 18 was harvested and immediately analysed with an LSM-510 laser scanning microscope (Carl-Zeiss, Jena, Germany) equipped with a Plan Neofluar 10•/0.3 objective or a C-Apochromat 40•/1.2 water objective (Behnke et al. 2010) to visualize the autofluorescence in leaf z-sections. Throughout the work, single-line excitation (UV laser 364 nm) and multiplechannel emission were used. For visualization of multispectral image data, the different channels were associated with a colour value on the display system [red, green, blue (RGB) colour mode]. The three simultaneously measured fluorescence channels were assigned to the primary display colours – 'pseudo-colours' – red [long-pass filter (LP), >560 nm], green [band pass filter (BP), 505–530 nm] and blue (BP 385-470 nm). Grey scale data (0-255, 0 = black and 255 = white) used for quantification of autofluorescence of phenolic compounds (blue and green channel) and for chlorophyll fluorescence (red channel) intensity were obtained by averaging fluorescence data from epidermal, first and second mesophyll cells of z-images monitored with identical cLSM parameter settings (for more details see Hutzler et al. 1998). Grey scale intensities were analysed with the LSM 5 Image Browser (Carl-Zeiss).

Determination of anthocyanins

Freshly harvested leaves were shock frozen in liquid nitrogen and stored at -80 °C, for further analysis. The material was homogenized in a mortar under liquid nitrogen to a fine powder. Aliquots of approximately 50 mg were extracted in an exactly 10-fold volume (w/v) methanol [high-performance liquid chromatography (HPLC) grade] at 4 °C overnight. For RP-HPLC analysis, 75 mL extract was mixed with 25 mL pure H₂O. Precipitated lipophilic material was removed by centrifugation for 10 min at 9000 g, and 10 mL aliquots of supernatant were immediately analysed by HPLC (Beckman HPLC System Gold, Beckman, Munich, Germany; column 250 × 4.5 mm Spherisorb ODS column (NC, 5 mm, Bischoff, Leonberg, Germany, at 20 °C, and a flow rate of 1 mL min⁻¹) as described in Ghirardo et al. (2012). The following solvents were used for gradient elution: solvent A [980 mL H₂O plus 20 mL 5% ammonium formate in formic acid (98%, w/v)] and solvent B [882 mL methanol plus 96 mL H₂O plus 20 mL ammonium formate in formic acid (98%, w/v)]. The gradient applied was 0-5 min, 100% A (isocratic); 5-45 min, 0-100% B, 45-48 min, 100% B, 48-58 min 100-0% B and 58-60 min 100% A. Detection was at 280 nm with a UV/visible diode array detector (Beckman Model 168).

Gas exchange and isoprene emission measurements

Gas exchange analysis was performed using a portable gas exchange system GFS-3000 (Walz, Effeltrich, Germany). In vivo measurements were performed at mid-day on leaf number 9 counted from the apex of the stem. An 8 cm² area

of the leaf was clamped into the gas exchange cuvette of the GFS-3000 and exposed to a flux of synthetic air (80% N₂, 20% O₂ and 380 ppm CO₂). The clamped leaf area was exposed to an incident PAR intensity of 1000 μ mol m⁻² s⁻¹, a relative humidity of 60% and the leaf temperature was set to 30 °C. Photosynthesis and isoprene emission rates were allowed to reach steady state (45 min) before recording values as means of 60 s.

Online, in vivo isoprene emission was measured at m/z 69 [(M + H)] by PTR-MS [Ionicon, Innsbruck, Austria (Hansel et al. 1995)] diverting a small air flux from the GFS-3000 cuvette outlet air to the inlet of the PTR-MS.

The PTR-MS was operating similarly as described in Ghirardo et al. (2011, 2012) with parameters E/N = 122.2 Td, the sum of contaminant ions O_2^+ , NO_2^+ and NO+ were less than 2%, H₃O·H₂O+ clusters were less than 5% of total primary ions. PTR-MS calibration was performed daily with a 10.9 ppmv isoprene standard in N₂ (Messer, Griesheim, Germany). The gas standard was diluted into the inlet air of the GFS-3000 and flushed through the empty cuvette at the beginning of the experiments with a flow rate of 0-50 mL min⁻¹.

Determination of photosynthetic pigments

Total chlorophyll content was determined according to Sims & Gamon (2002). For determination of carotenoid composition, 100% acetone extracts were separated and quantified by HPLC (PerkinElmer; series 200 Pump, Rodgau, Germany) following the method of Thayer & Björkman (1990) and as described by Haldimann et al. (1995). Pigments from acetone extracts were separated using Alltima C18 column $(250 \times 4.6 \text{ mm}, 5 \mu\text{m} \text{ particle size by Alltech Italia Srl},$ Bologna, Italy). A total of 40 µL of acetone extract was injected and the pigments were eluted using 100% solvent A (acetonitrile: methanol, 85:15) from 0 to 13 min, 100% solvent B (methanol: ethylacetate, 68:32) from 13 to 20 min, and 100% solvent C (methanol: ethylacetate, 50:50) from 20 to 25 min. Finally, the column was re-equilibrated with solvent A for 5 min, prior the next injection. The temperature of the column was adjusted at 26 °C and the flow rate at 1.1 mL min⁻¹. The pigments were detected by their absorbance at 445 nm. Peak areas were integrated by the PerkinElmer Spectrophotometer detector (LC-95 UV/visible). The amount of any pigment was calculated from the integrated area of the corresponding peak. The de-epoxidation state of the xanthophylls was calculated as (0.5 A + Z)/(A + Z + V), where A is antheraxantin, Z is zeaxanthin and V is violaxanthin.

Non-targeted metabolome analysis

From each sample, 5 mg of powdered leaf material was extracted with 1 mL -20 °C extraction solvent [methanol/ isopropanol/water 1:1:1 (v/v/v)] in an ultrasonic bath for 15 min. Subsequently, the solution was centrifuged at 10 000 g for 10 min at 4 °C. The supernatant was removed and diluted with extraction solvent in a ratio of 1:12.5 (v/v).

For non-targeted metabolome analysis ultra-high-resolution mass spectra were acquired using a Fourier transform ion cyclotron resonance mass spectrometer (FT-ICR-MS, APEX Qe, Bruker, Bremen, Germany) equipped with a 12 Tesla superconducting magnet and an APOLLO II electrospray (ESI) source. Samples were introduced into the microelectrospray source (Agilent sprayer, Waldbronn, Germany) at a flow rate 120 μL h⁻¹ with a nebulizer gas pressure of 20 psi and a drying gas pressure of 15 psi at 200 °C by a Gilson autosampler (Sample changer 223, Gilson Inc., Middleton, WI, USA). All measurements were performed in the negative ionization mode over a mass range of m/z 100-1000. The spectra were acquired over a time domain transient of 2 Megawords with 438 accumulated scans for each sample. To exclude memory effects in the ICR cell, samples were randomized and the mass spectrometer was cleaned with Methanol between each run for 7 consecutive minutes.

The resulting mass spectra were internally calibrated and exported to peak height lists as ASCII files at a signal to noise ratio of 2 using the Data Analysis 4.0 software package (Bruker, Bremen, Germany). The peak lists were combined to a peak matrix with an error of 1.5 ppm using an in-house written tool (Lucio *et al.* 2011). Peaks with just 1 non-zero intensity (single mass events) were removed from the matrix as well as peaks that were detected in less than 50% of all biological replicates. After that, a 13C isotopic peak filter was applied, deleting peaks with no corresponding 13C isotopic peak to avoid signals generated by electrical noise. Overall, 4412 masses remained after all filtration processes.

Intensities were total ion current (TIC, sum of all intensities) normalized. Therefore, each peak intensity was divided by the sum of all intensities of the corresponding spectrum and multiplied by the average TIC of all measured sample spectrums [(Intensity(i)/TIC(i))*TIC(average)].

For metabolite identification, the masses were corrected for H+ loss and uploaded to the MassTrix 3 server selecting *P. trichocarpa* as organism (Suhre & Schmitt-Kopplin 2008), PoplarCyc database (Zhang *et al.* 2010), Knapsack database (Oikawa *et al.* 2006, Shinbo *et al.* 2006) and Metlin database (Smith *et al.* 2005) with a maximal error acceptance of 3 ppm.

Statistical analysis

For statistical analysis of the metabolomic data, the peak matrix containing the peak intensities was utilized as variables 'X' for principal component analysis (PCA) and partial least squares (PLS) regression using the software package The Unscrambler 8.0 (CAMO Software AS, Oslo, Norway). Before analysis, X-variables were centred and scaled to unit variance. Both PCA and PLS models were validated using full cross-validation. In addition, the stability of PLS models were assessed with the jack-knifing-based approach Martens Uncertainty Test (Martens & Martens 2000).

PCA was first employed to describe the metabolomic data in an objective and unsupervised manner. Then PLS was used to extract discriminant masses, which could significantly differentiate samples according to their isoprene emission ability (i.e. NE/IE) and time behaviour. Discriminant masses were discovered by means of Martens Uncertainty Test from PLS models type 2 calculated with two Y-variables, the first describing NE/IE (Y = 0/1), the second describing the different time points (Y = 0-6). Similarly, a second PLS model type 1 was calculated for the extraction of discriminant masses describing the applied UV treatment with one Y-variable UV-B-/UV-B+ (Y = 0/1). The fitness of a PLS model was measured by a regression between the measured- versus predicted-Y-scores. Slopes and coefficient of determinations (R^2) of those regressions were always >0.91 and >0.96 for calibration models, and >0.82 and >0.92 for the validation models, respectively.

Time behaviour of discriminant masses was investigated using the Profile Search function of the Hierarchical Clustering Explorer (HCE v3.5; http://www.cs.umd.edu/hcil/hce/), with Pearson's r > 0.85 as distance measure. Two-way analysis of variance (ANOVA) with Fisher's least significant difference (LSD) test (P < 0.05) was used for the calculation of significant differences in the HPLC data. To ensure statistical differences of the cLSM data, one-way repeated-measures anovas with Bonferroni t-tests (P < 0.05) were used (Sigmaplot 12.0, Systat Software Inc., San Jose, CA, USA).

RESULTS

Measurement of phenolic compounds uncovers differential accumulation of UV-absorbing pigments upon UV-B exposure

We observed different visible phenotypes of IE and NE plants grown under control and UV-B conditions (Fig. 1a). This conspicuous visual differentiation was observable with the formation of different leaf colours after 13 d of UV-B exposure and indicated different accumulation of leaf pigments among the poplar genotypes. We quantified leaf pigments via HPLC, starting with the quantification of two anthocyanidin equivalents derived from cyanidin. Summing up the concentration of both anthocyanidins, we observed an increase in concentration over the experimental time course (Fig. 1b,c), which reached up to a 2.7-fold higher concentrations in UV-B exposed leaves compared with controls. These changes were significant (ANOVA, Fisher's LSD, P < 0.001) after 5 d of UV-B exposure. In contrast, to the clear visible difference in red coloration of the leaves (Fig. 1a) related to UV-B exposure and genotype, the analysis of anthocyanidins revealed only significant lower concentrations (P < 0.001) in UV-exposed NE poplars compared with IE poplars at day 5 of the experiment. Analysis of phenolic compounds showed different concentration patterns between control and UV-exposed leaves. The concentration of quercetin-3rhamnoside, a flavonol glycoside (retention time: 31.7 min) increased steadily with time and was significant higher (P < 0.001) after 5 d of UV exposure (Fig. 1d,e). Furthermore, we observed significant lower concentrations in NE plants at days 2 and 5. In contrast to the steadily increasing quercetin 3-rhamnoside, the concentration of the coumaric acid derivative, eluting at 25.8 min, decreased by 50-60% within the first 2 d of UV-B exposure (Fig. 1f,g). Concentration differences between UV-exposed and control plants

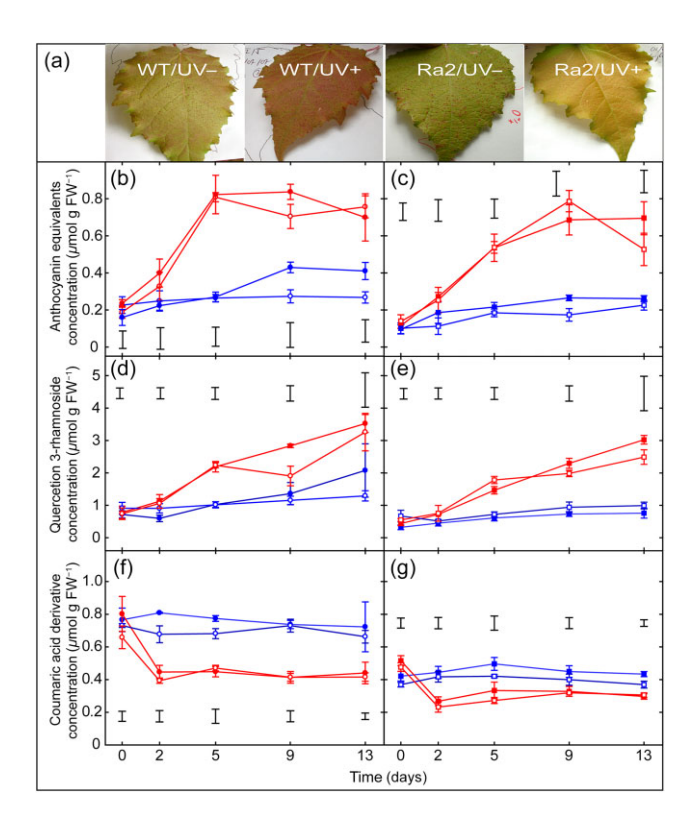


Figure 1. (a) Emerging phenotype after 13 d of UV-B exposure. Anthocyanin concentration (sum of cyanidin and cyanidin glucoside) in poplar leaves followed over the course of the experiment via high-performance liquid chromatography (HPLC) of (b) control isoprene-emitting (IE) poplar and UV-B-exposed IE poplars, plus the concentration in leaves of (c) control non-isoprene-emitting (NE) poplar lines and UV-B-exposed NE lines, normalized to nmol cyanin g⁻¹ fresh weight. The concentration of quercetin-3-rhamnoside for (d) control and UV-B-exposed IE poplars and (e) of control and UV-B-exposed NE poplars. Time course of a coumaric acid derivative in (f) IE poplars and (g) NE poplars. The values represent the means of 4 biological replicates ± SE. Bars in the figure indicate least significant difference (LSD) values [analysis of variance (ANOVA), Fisher's LSD test] WT/UV-, ---; EV/UV-, ---; WT/UV+, ---; EV/UV+, ----; Ra2/UV-, ------; Rb7/UV-, ------; Ra2/UV+, -------; Rb7/UV+, -□-.

were significant after 2 d of UV-B treatment (ANOVA, P < 0.001). Additionally, ANOVA analysis revealed also differences between control NE and IE plants (P < 0.05), but only a significant reduced concentration (P < 0.05) in UV-exposed NE compared with IE poplars at days 2 and 5.

cLSM of leave z-sections reveals varying light penetration depth

Analysis of auto-fluorescence (excited at 364 nm) in z-sections of leaf surfaces indicated a varying depth of light penetration into the adaxial leaf surface depending on plant type and UV-B treatment (Fig. 2a). Exposure of plants to UV-B resulted in a strong quenching of UV-induced autofluorescence in epidermal and the next adjacent mesophyll cells compared with controls. The quenching was less pronounced in NE than IE lines. In particular, ANOVA analysis of cell-specific grey scale intensities showed significant differences between UV-treated and control WT leaves (P < 0.001, Fig. 2b,c), and between UV-exposed IE and NE leaves in the first two cell layers of the blue and green channel (P < 0.001, Fig. 2b,c), along with the differentiation of WT and Ra/UV ± leaves in the first two layers of the blue channel (P < 0.001, Fig. 2b,c). However, ANOVA analysis did not show significant differences between UV-exposed NE and control NE plants (P = 0.054).

Marginal effects of UV-B radiation on photosynthesis and isoprene emission

To identify UV-B effects on leaf xanthophyll contents, the total concentration of xanthophylls was measured and the xanthophyll/chlorophyll a (Chl a) ratio was calculated. A shift towards higher xanthophyll content in all lines under UV-exposure was observed (Supporting Information Fig. S3a,b). These changes were significant in IE poplars at day 5 of UV exposure (WT: P < 0.001, EV: P = 0.016) and in NE lines at day 9 (Ra: P = 0.015, Rb: P = 0.02).

The carotenoid/Chl a ratio increased throughout the experiment and showed a tendency towards higher carotenoid content in UV-exposed IE plants until day 9 (Supporting Information Fig. S3c,d). However, we observed no significant differences in the carotenoid ratios and in the de-epoxidation ratio (Supporting Information Fig. S3e,f).

Gas exchange analysis did not reveal significant changes in net CO₂ assimilation rates during UV-exposure in IE

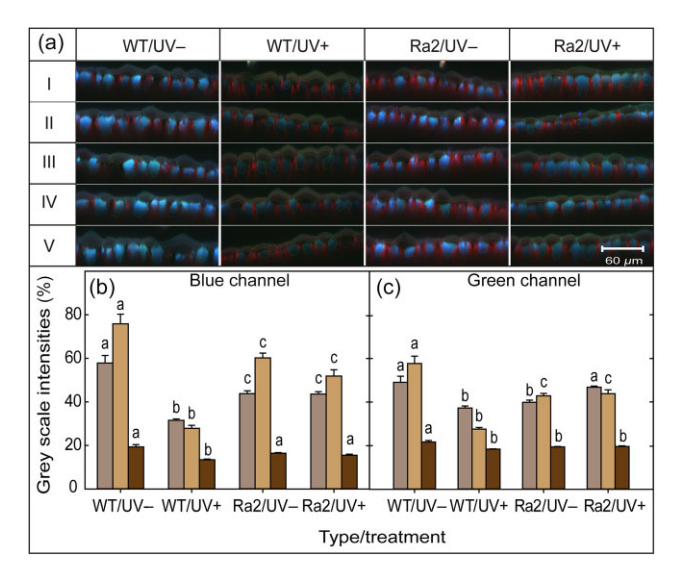


Figure 2. (a) Confocal laser scanning microscopy images of leaf's z-sections (leaf no. 18) from five biological replicates (I–V) taken after 13 d of UV-B treatment and their grey scale intensities in the (b) blue and (c) green channel of the epidermal cell layer (■), the first mesophyll cell layer () and the second mesophyll cell layer (\blacksquare). Values represent the mean over five measurements \pm SE. Bars with varying letters indicate significant differences between lines and treatments [P < 0.05, analysis of variance (ANOVA) with Bonferroni *t*-tests].

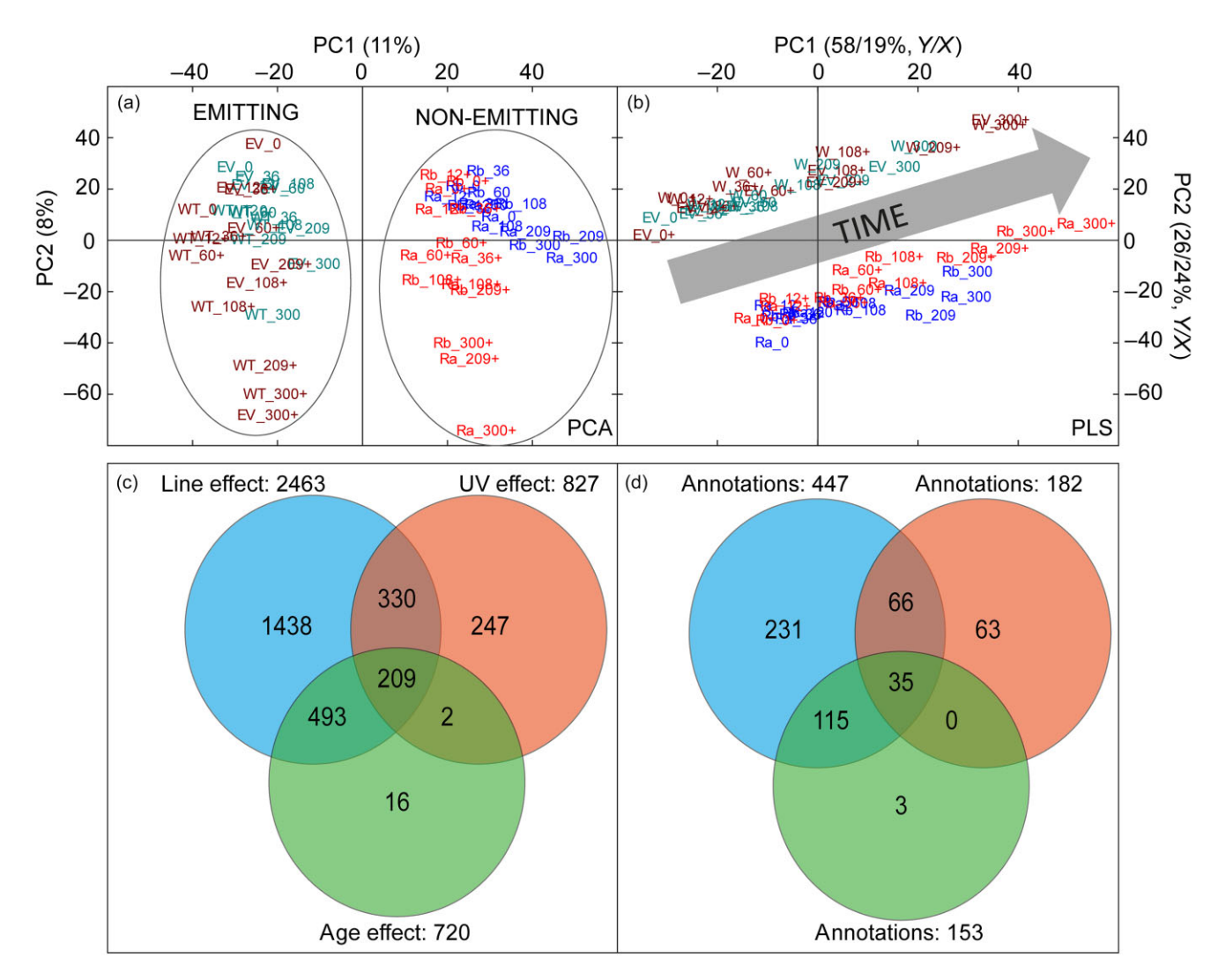


Figure 3. Score plots of (a) principal component analysis (PCA) from Fourier transform ion cyclotron resonance mass spectrometry (FT-ICR-MS) metabolomic data and (b) partial least squares regression (PLS, calibration: slope = 0.97, $R^2 = 0.99$ validation: slope = 0.94; $R^2 = 0.98$). Colours represent the different poplar lines and treatment conditions [WT/EV-UV-(\blacksquare), WT/EV-UV+(\blacksquare)]. Numbers behind symbols indicate the respective sampling time in hours (h). Venn diagrams of (c) discriminant masses arranged to their correlated experimental *Y*-variable. (d) Visualization of the total number of annotations. Colours indicating the different experimental variables, masses, are discriminant for line effect (\blacksquare), ultraviolet radiation (UV) effect (\blacksquare) and time behaviour (\blacksquare). PC1, PC2, principal components 1, 2; X, Y, explained X-, Y-variance.

poplars (Supporting Information Fig. S4a). The NE lines responded to UV-B radiation with a decrease of net CO_2 assimilation ranging from 22 to 37% betweens days 1 and 9, with significant differences at day 9 (P = 0.02), followed by an immediate recovery at day 13 (Supporting Information Fig. S4b).

We observed a clear tendency towards lower isoprene emission rates under UV-B exposure, which were most prominent at day 13 (Supporting Information Fig. S4c,d). Changes in transpiration rates between NE and IE as well as between UV-exposed and control plants were not observed (Supporting Information Fig. S4e,f). Concurrently, we also observed no difference in stomata conductance under UV-B exposure (Supporting Information Fig. S5).

Non-targeted metabolomics reveals severe metabolic rearrangements related to UV-B treatment and genetic background

PCA of metabolomic data revealed a distinct clustering of IE and NE plants in the first component of the PCA score plot, explaining 11% of total variance (Fig. 3a). UV-B-treated plants separated from control plants after 108 h in IE plants and after 60 h in NE poplars in principal component 2 (PC2) interpreting 8% of total variance. Additionally, the PCA score plot recorded a clear time trend of the metabolome data in PC2 that was present in all genotypes.

To exclude ageing effects, a separate PLS model, independent of the UV and line variables, was used (Fig. 3b),

explaining a total of 84% Y-variance within the first two components and having a slope of 0.89 and correlation coefficient of 0.98 between measured and predicted Y of the validation set of samples.

Overall, we found 2735 discriminant masses and correlated them to their respective experimental variable (Fig. 3c). 2463 masses were discriminant for the separation of IE from NE plants, 827 masses were discriminant for the UV treatment and 720 masses were responsible for the separation of time points, which describe plant ageing (Fig. 3c). Overall, only 513 (18.76%) masses could be annotated as metabolites through databases (Fig. 3d). Metabolic differences between NE and IE poplars ranged over various pathways of primary and secondary metabolism including carbohydrate, energy, lipid, nucleotide, amino acid, phenolic, terpenoid, vitamin and cofactor metabolism (Supporting Information Fig. S6). These pathways were also affected in leaves of UV-exposed plants, whereby the majority of annotated metabolites (70.6%) were either phenolic compounds or steroids. Only few metabolites belonged to carbohydrate, amino acid, energy or terpenoid metabolism (Supporting Information Fig. S7).

Since the PCA score plot indicated a distinct time trend of the metabolome data, we focused on time series analysis. We observed that plenty of the discriminant masses (1287) gathered in four different profiles (Fig. 4). The first two profiles indicate line-dependent metabolic differences that existed during control and UV-B conditions and whose peak intensities stayed constant throughout the experiment (Fig. 4a,b). The first cluster included 604 masses that were up-regulated in NE plants (Fig. 4a) and the second cluster contained 368 metabolites with higher peak intensities in IE poplars (Fig. 4b). We found relative higher contents of terpenes and carbohydrates in NE than in IE plants, especially metabolites of the terpenoid and terpenoid backbone biosynthesis, such as dimethylallyl diphosphate, which is the biosynthetic precursor of isoprene, geranyl-geranyl monophosphate, gibberellin A8-catabolite, gibberellin A28, gibberellin glucoside, ubiquinone, farnesyl pyrophosphate monophosphate, were up-regulated in NE lines. Additionally, many annotated metabolites of the first two clusters were phenolics such as flavonoids, polyphenols and phenylpropanoids. These line-dependent accumulation patterns of phenolic compounds were conserved upon UV-B exposure.

Looking specifically for changes in metabolite levels that occur under UV-B radiation, we found two key profiles: (1) metabolites that were UV-induced (Fig. 4c) and (2) metabolites whose concentration was decreasing within the first 12 h of UV-B treatment (Fig. 4d). Annotated UV-B-induced metabolites were mainly (87%) flavonoids, phenylpropanoids and phenolic glucosides, whereas cluster four contained steroids and vitamin D2 derivatives.

Most of the annotations for UV- and line-dependent discriminant masses belonged to plant phenolics. Thus we focused on flavonoid and phenylpropanoid metabolism, observing line-dependent regulatory processes (Fig. 5). IE and NE poplars may choose alternative biosynthetic routes leading to phenylpropanoids, either via phenylpyruvate or via 4-hydroxyphenylpyruvate, which are the biosynthetic precursor of Phe and Tyr, respectively. IE poplars exhibited slightly higher amounts of phenylpyruvate, whereas NE lines showed a higher content of 4-hydroxyphenylpyruvate (Fig. 5).

We found a similar trend for both coniferin and syringin levels. NE poplars seem to prefer coniferin whereby IE poplars show a preference for syringin. These trends also exist in the flavonoid pathway proper. IE lines selected the biosynthetic route to hesperidin for flavanone production while NE lines preferred the direction leading to naringin. Furthermore, in leaves of IE plants, flavonoids used for anthocyanine biosynthesis were up-regulated and simultaneously gallocatechin and catechin, which are precursors for proanthocyanidins, were down-regulated. NE lines also induced flavone biosynthesis as seen by higher content of apigenin, luteolin, vitexin and their biosynthetically modified derivatives (Fig. 5). Methylated and glucosylated flavones were also UV-induced, whereas acetylated apigenin derivatives were down-regulated. An effect of UV radiation on intermediates of flavonoid biosynthesis was hardly seen. UV radiation rather caused a change on biosynthetic endproducts and polyphenols.

DISCUSSION

First-time UV-B exposure of UV-free cultivated NE and IE grey poplars (Populus × canescens), resulted in genotype dependent leaf colour development. This lead to a diminished light transmission through epidermis of UV-exposed NE leaves compared with treated IE leaves after 13 d of UV-B irradiation. Non-targeted metabolomics elucidated the time-dependent accumulation of phenolic compounds with line-dependent differences. Additionally, the non-targeted approach revealed a quick down-regulation of steroid derivatives in IE and NE poplar plants exhibiting a possible crosstalk between phenolic and terpenoid biosynthesis.

The formation of different leaf colour phenotypes allowed us to visually distinguish between NE and IE plants after 13 consecutive days of UV-B treatment. Leaf colour changes result from alterations of leaf pigment concentrations, for example, anthocyanins, carotenoids, xanthophylls and chlorophylls (Tanaka et al. 2008). Particularly, anthocyanins are responsible for a red leaf colour by their accumulation in leaf vacuoles, during autumn leaf senescence. These compounds protect against high light intensities at low temperatures (Chang et al. 1989; Hoch et al. 2003). Earlier work on redleafed plants also revealed high contents of colourless phenolic compounds, which contribute more than anthocyanins to the overall absorbance of UV radiation (Woodall & Stewart 1998).

The analysis of plant phenolics revealed different distribution patterns between control and UV-exposed and between NE and IE plants supporting the hypothesis of genotype- and treatment-dependent phenolic distributions. Accumulation of flavonoids under UV-B radiation is well documented in literature (Schnitzler et al. 1996; Lavola 1998; Lake et al. 2009) and is in agreement with our findings of increasing

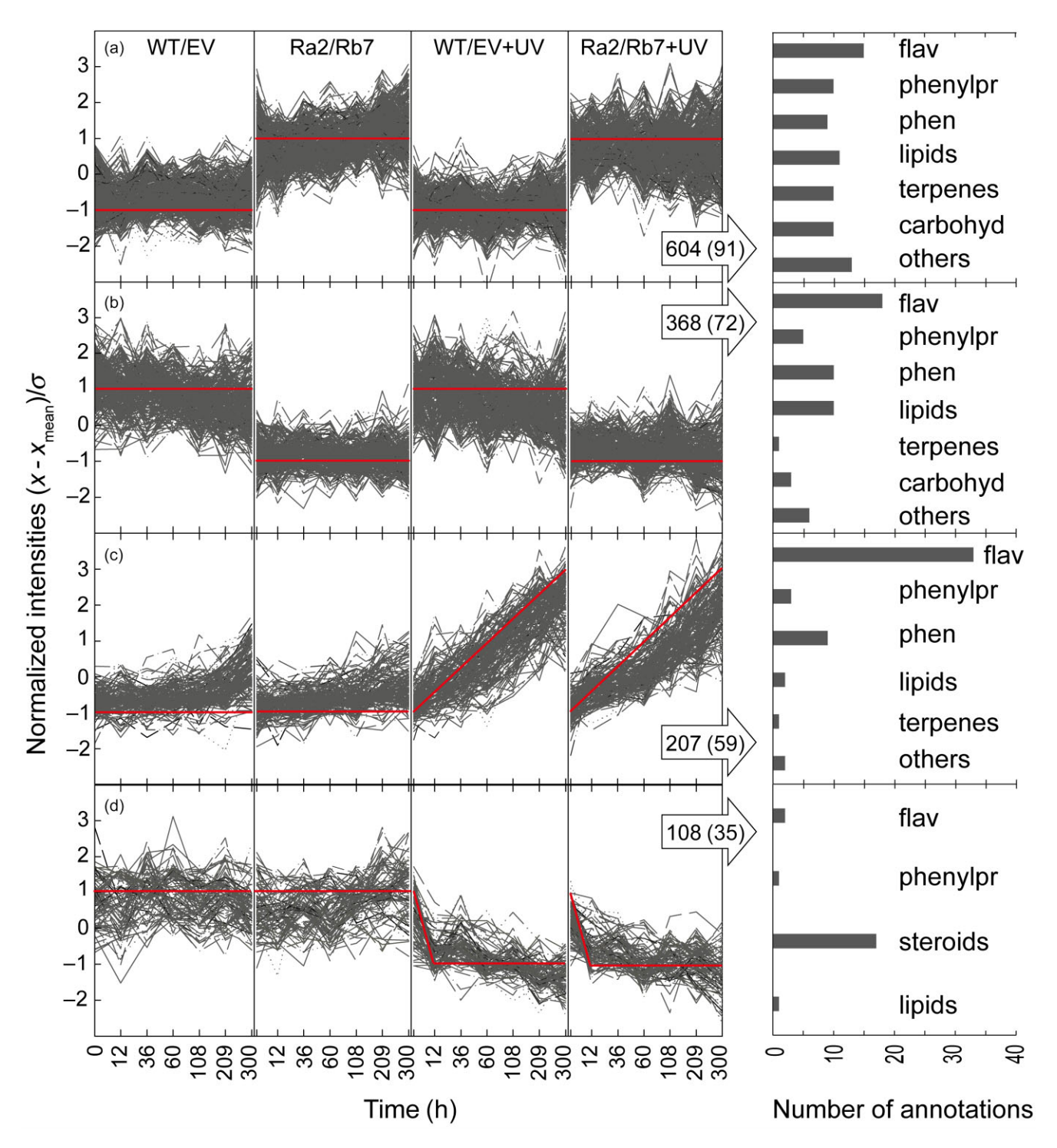


Figure 4. Time behaviour of normalized signal intensities $\{x$ -axis = $[(x - x_{\text{mean}})/\sigma]$, y-axis = time [d] $\}$ from discriminant masses in four major time clusters: up-regulated metabolites in (a) non-isoprene-emitting (NE) (Ra2/Rb7), (b) in isoprene-emitting (IE) (WT/EV), (c) metabolites induced under UV-B irradiation and (d) metabolites decreasing within the first 12 h of UV-B exposure. Red lines indicate the time profile entered into the profile search function of Hierarchical Clustering Explorer (HCE) 3.5 and grey lines indicate masses, which matched the entered profile. The number of masses within a cluster is given in the arrows. Numbers in brackets stand for the amount of annotations. The annotations were grouped into compound classes and visualized in bar plots. carbohyd, carbohydrates; flav, flavonoids; phen, phenolic; phenylpr, phenylpropanoids.

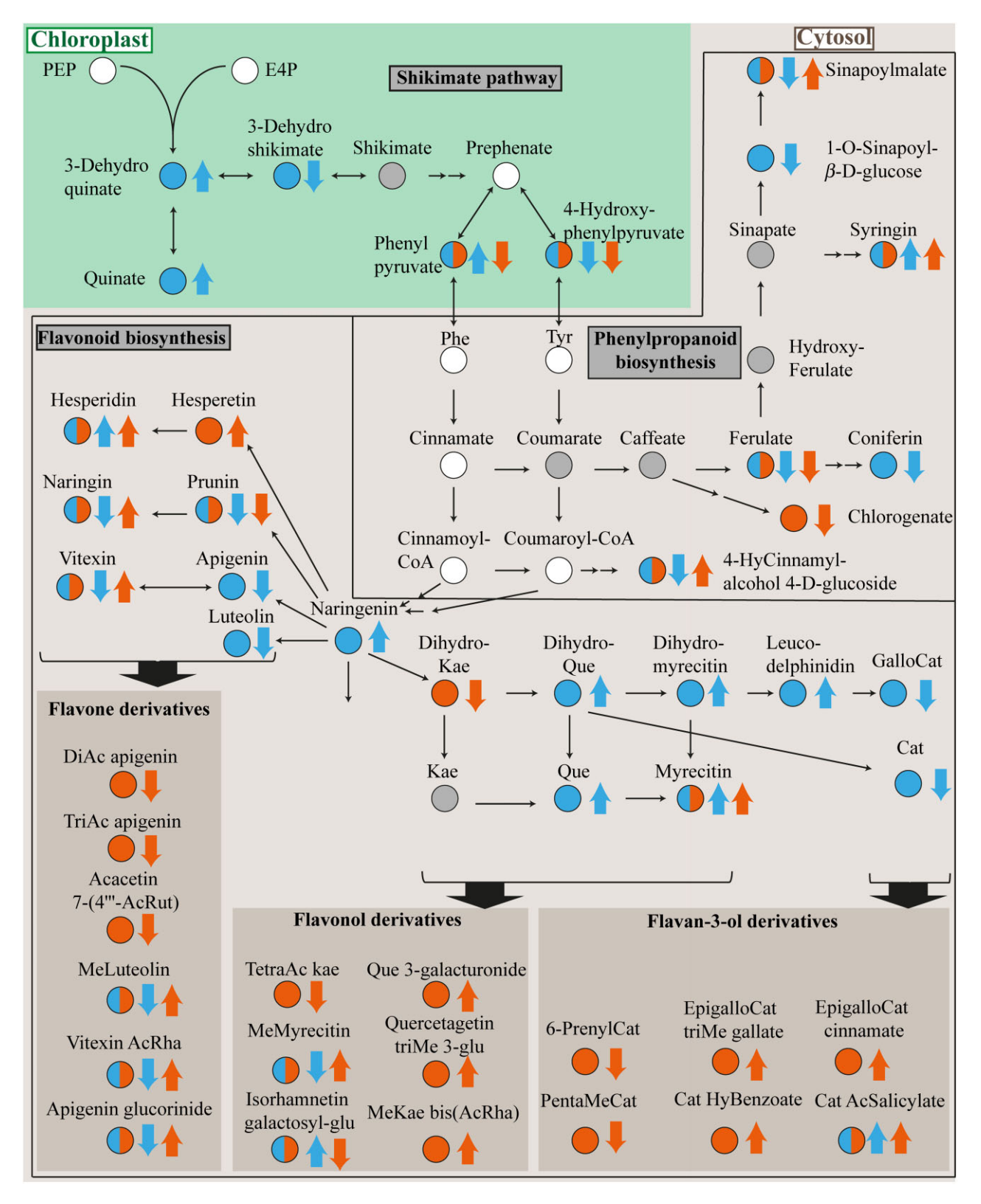


Figure 5. Map of the shikimate pathway, phenylpropanoid and flavonoid biosynthesis and their respective compartmentalization. Blue colour on indicates line-dependent significant changes and red colour indicates significant changes due to UV irradiation. Metabolites, discriminant for both experimental variables, hold both colours . Non-identified metabolites appear white \bigcirc and identified but not discriminant metabolites appear grey . The coloured arrows indicate up- and down-regulation [up-regulated in isoprene-emitting (IE) and ↓ down-regulation in IE, ↑ up- and ↓ down-regulation under ultraviolet radiation (UV)]. Ac, acetyl; Cat, catechin; glu, glucose; Hy, hydroxy; Kae, kaempferol; Me, methoxy; Que, quercetin; Rha, rhamnoside; Rut, rutenoside.

Additionally, the microscopical results of UV-treated NE poplars demonstrated a reduced production and accumulation of UV-B absorbing compounds in epidermal tissue evidenced by the curtailed light transmission compared with controls and IE poplars. This reduced accumulation of UV-absorbing compounds might be linked to the isoprenereduced poplar phenotype and a successive reorganization of signalling processes involving isoprene.

Up to now, five different photoreceptors perceiving light at different wavelengths are known (Jiao et al. 2007; Rizzini et al. 2011; Lau & Deng 2012). The phytochromes (phyA and phyB) and cryptochromes (cry1 and cry2) sense visible light and suppress CONSTITUTIVE PHOTOMORPHOGENIC PROTEIN 1 (cop1), which is the repressor of photomorphogenesis (von Arnim & Deng 1994; Lau & Deng 2012). Under UV-B radiation, however, cop1 is directly regulated by the UV-B receptor UVR8. They jointly active the transcription factor LONG HYPOCOTYL 5 (HY5), which in turn activates the MYB (myeloblastosis) transcription factors (TFs; Gonzalez et al. 2008; Lau & Deng 2012; Shin et al. 2013). Four of those TFs (MYB75, MYB90, MYB113 and MYB144) code directly for anthocyanine biosynthesis. It has been shown that MYBs can be controlled by changes in the cellular redox potential (Heine et al. 2004; Dubos et al. 2010) and H₂O₂ levels (Vanderauwera et al. 2005).

Since, earlier analysis of NE poplars showed an accumulation of H₂O₂ *in vivo* compared with IE plants it might be speculated that the higher amount of this ROS species influence the regulatory network at the MYB stage resulting in different pheno(chemo)types. Indeed, earlier transcriptomic analysis (Behnke *et al.* 2010) demonstrated a downregulation of MYB or MYP-like TFs (orthologs of AtTTG1, coding for a WD40 protein, AtMYB4, AtMYB58) in NE poplars that coincided with reduced proanthocyanidin accumulation.

Our non-targeted metabolome analysis revealed an up-regulation of flavonoids used for anthocyanin biosynthesis in IE poplars (Fig. 5) and simultaneously a down-regulation of gallocatechin and catechin, which are important precursors for proanthocyanidin biosynthesis (Winkel-Shirley 2001; Koes *et al.* 2005). Proanthcyanidins can either be colourless or brown, whereas vacuolar anthocyanins are typically red (Koes *et al.* 2005). This fact,

together with the observed diverse activation of anthocyanin and proanthocyanidin pathways, may explain the development of phenotypic differences after treating IE and NE poplar with UV-B radiation.

Furthermore, UV-B radiation triggered the production of catechin and epicatechin-based polyphenolic compounds connected to a galloyl residue, also known as theaflavins (Quideau *et al.* 2011). The hydroxybenzoic acid moieties, to which the flavan-3-ols are connected, hold an absorption maxima within the UV-B range (280–320 nm), promoting them to perfect UV-absorbing pigments (Pietta 2000; Quideau *et al.* 2011). Key characteristics of polyphenols also include their direct quenching ability of radical ROS species (Pietta 2000; Zhou *et al.* 2005; Quideau *et al.* 2011). Inducing the production of theaflavins and theaflavin-like compounds by UV-B radiation lessened the metabolite levels of methylated and prenylated catechin derivatives backing up the enhanced production of theaflavins for increased UV protection (Fig. 5).

UV-B radiation also triggered line-dependent changes in flavonol and flavone biosynthesis, leading towards up- and down-regulation of flavonol and flavone derivatives. These compounds are mainly methylated, acetylated or possess a glycan moiety. O-methylations and acetylations increase lipophilicity (Ibrahim et al. 1987; Harborne & Williams 2000; Zhou et al. 2006). Furthermore, O-methylations blue-shift the absorption maxima, typically to the 250-320 nm region (Harborne & Williams 2000). A boost in lipophilicity facilitates the embedment into biomembranes (Brisson et al. 1986; Charest et al. 1986) and affects compartmentalization (Zhou et al. 2006). The epidermal tissue is known to be responsible for cuticle wax layer formation, protecting leaves against water loss (Riederer & Schreiber 2001). We speculate that an increase in lipophilicity of flavonoid end-products is correlated with transportation processes leading towards the embedment of flavonoids into cell walls of the epidermal tissue or chloroplasts, where they also can quench singlet oxygen (Agati et al. 2007). Furthermore, NE lines favoured the production of flavones compared with IE poplars.

We also observed line-dependent UV-B changes in aromatic amino acid metabolism. Phenylpyruvate and 4-hydroxyphenylpyruvate, which are synthesized through the chloroplastidic shikimate pathway, were both downregulated in UV-exposed plants (Fig. 5). This could either indicate an increase in 4-hydroxyphenylpyruvate aminotransferase (HPP-AT) and phenylpyruvate aminotransferase (PPY-AT) activities or a preference towards biosynthesis of phenylalanine (Phe) and tyrosine (Tyr) via arogenate. Both explanations lead to an increase of Phe and Tyr production, the key metabolites for phenylpropanoid biosynthesis. Changes in phenylpropanoid metabolite levels caused by UV-B radiation were mainly visible on biosynthetic end-products such as sinapoyl malate, chlorogenate and 4-hydroxycinnamyl alcohol 4-D-glucose (Fig. 5). Sinapate esters like sinapoyl malate are known to exhibit major functions in UV-B protection (Li et al. 1993; Landry et al. 1995). In UV-exposed flavonoid deficient Arabidopsis mutants, an accumulation of sinapoyl malate has been observed to compensate the lack of flavonoids (Landry et al. 1995; Kusano et al. 2011). IE poplar leaves have higher content of syringin, but exhibit lower contents of coniferin. Both of them are used for the biosynthesis of lignins, so it might be speculated whether these differences influence lignin composition of leaves. Indeed, wood composition analysis (Behnke et al. 2012) showed low concentration of syringyl lignin in NE plants compared with IE (Behnke et al. 2012). Interestingly, we observed an immediate downregulation of steroid levels upon UV-B radiation (within 12 h), which is in contrast to previous work on Vitis vinifera L. leaves (Gil et al. 2012), where authors reported an up-regulation of membrane-related steroids. Phenolic metabolism and steroid biosynthesis are linked by the central biosynthetic intermediate phosphoenolpyruvate (PEP; Dizengremel et al. 2012). PEP can either be converted to pyruvate, which represents the entry point of the MEP pathway, by pyruvate kinase (PK), or it is used for the biosynthesis of phenolic compounds through the shikimate pathway, to which up to 30% of photosynthetically fixed carbon is directed (Razal et al. 1996; Huang et al. 2010; Maeda & Dudareva 2012). The carbon flux through the MEP pathway is mainly used for isoprene synthesis (Sharkey & Yeh 2001; Li & Sharkey 2013). The down-regulation of steroid contents followed by the tendency of lower isoprene emissions rates under UV-B radiation might be a regulatory step in adjusting metabolic fluxes in the direction of phenolic biosynthesis, facilitating UV adaption in poplar. During this rearrangement, the PEP/pyruvate balance, which is controlled by PK activity, may determine the process of UV adaption. The absence of isoprene emission eventuates in C-flux changes through the MEP pathway and therefore alters the biosynthesis of phenolic compounds in NE poplars under control and UV conditions.

In summary, the present comprehensive metabolomic analysis of UV-induced overall metabolic shifts in isoprene and non-isoprene-emitting poplar revealed remarkable metabolome-wide transient adjustments of pathways resulting in differentially colour phenotypes of IE and NE poplars. The clear and very distinct metabolic differences in the accumulation and composition of the poplar 'phenolic metabolome' pave the way for a detailed analysis of the underlying regulatory network of transcription factors (i.e. MYBs) and the indicated interferences of isoprene on it. Moreover, the deciphered pleiotropic differences in metabolite profiles among emitter types, UV-B radiation, salt stress (Behnke et al. 2013) and different atmospheric CO₂ (Way et al. 2013) will form the mechanistic base to understand the different sensitivity of IE and NE poplars to fungal disease and herbivory (Behnke et al. 2012) found in a 2 year field trail with these lines.

ACKNOWLEDGMENTS

The study was financially supported by the Human Frontier Science Program (HFSP, to J.-P.S.), an exchange grant from the European Science Foundation (ESF) within the scientific programme 'VOCBAS' (to C.B.) and the EU COST Action FA0906 UV4Growth (A.A. and J.B.W.).

REFERENCES

- Agati G., Matteini P., Goti A. & Tattini M. (2007) Chloroplast-located flavonoids can scavenge singlet oxygen. The New Phytologist 174, 77-89.
- Agati G., Azzarello E., Pollastri S. & Tattini M. (2012) Flavonoids as antioxidants in plants: location and functional significance. Plant Science 196, 67-76.
- Aharoni A., Ric de Vos C.H., Verhoeven H.A., Maliepaard C.A., Kruppa G., Bino R. & Goodenowe D. (2002) Nontargeted metabolome analysis by use of Fourier transform ion cyclotron mass spectrometry. Omics: A Journal of Integrative Biology 6, 217-234.
- von Arnim A.G. & Deng X.-W. (1994) Light inactivation of arabidopsis photomorphogenic repressor COP1 involves a cell-specific regulation of its nucleocytoplasmic partitioning. Cell 79, 1035–1045.
- Behnke K., Ehlting B., Teuber M., Bauerfeind M., Louis S., Hasch R. & Schnitzler J.P. (2007) Transgenic, non-isoprene emitting poplars don't like it hot. The Plant Journal 51, 485-499.
- Behnke K., Kaiser A., Zimmer I., Bruggemann N., Janz D., Polle A. & Schnitzler J.P. (2010) RNAi-mediated suppression of isoprene emission in poplar transiently impacts phenolic metabolism under high temperature and high light intensities: a transcriptomic and metabolomic analysis. Plant Molecular Biology 74, 61-75.
- Behnke K., Grote R., Bruggemann N., Zimmer I., Zhou G.W., Elobeid M. & Schnitzler J.P. (2012) Isoprene emission-free poplars - a chance to reduce the impact from poplar plantations on the atmosphere. New Phytologist 194,
- Behnke K., Ghirardo A., Janz D., Kanawati B., Esperschuetz J., Zimmer I. & Rosenkranz M. (2013) Isoprene function in two contrasting poplars under salt and sunflecks. Tree Physiology 33, 562-578.
- Brisson L., Vacha W.E.K. & Ibrahim R.K. (1986) Localization of partially methylated flavonol glucosides in Chrysosplenium americanum. II. Immunofluorescence, Plant Science 44, 175-181.
- Britt A.B. (1995) Repair of DNA damage induced by ultraviolet radiation. Plant Physiology 108, 891-896.
- Brüggemann N. & Schnitzler J.P. (2002) Comparison of isoprene emission, intercellular isoprene concentration and photosynthetic performance in water-limited oak (Quercus pubescens Willd. and Quercus robur L.) saplings. Plant Biology 4, 456-463.
- Burchard P., Bilger W. & Weissenböck G. (2000) Contribution of hydroxycinnamates and flavonoids to epidermal shielding of UV-A and UV-B radiation in developing rye primary leaves as assessed by ultravioletinduced chlorophyll fluorescence measurements. Plant, Cell & Environment 23, 1373-1380.
- Caldwell M.M. (1971) Solar UV irradiation and the growth and development of higher plants. In Photophysiology, Vol. 6 (ed. A.C. Giese), pp. 131-177. Academic Press, New York.
- Caldwell M.M., Bornman J.F., Ballare C.L., Flint S.D. & Kulandaivelu G. (2007) Terrestrial ecosystems, increased solar ultraviolet radiation, and interactions with other climate change factors. Photochemical & Photobiological Sciences 6, 252-266
- Carletti P., Masi A., Wonisch A., Grill D., Tausz M. & Ferretti M. (2003) Changes in antioxidant and pigment pool dimensions in UV-B irradiated maize seedlings. Environmental and Experimental Botany 50, 149-157.
- Chang K.-G., Fechner G.H. & Schroeder H.A. (1989) Notes: anthocyanins in autumn leaves of quaking aspen in colorado. Forest Science 35, 229-236.
- Charest P.M., Brisson L. & Ibrahim R.K. (1986) Ultrastructural features of flavonoid accumulation in leaf cells of Chrysosplenium americanum. Protoplasma 134, 95-101.
- Costa H., Gallego S.M. & Tomaro M.L. (2002) Effect of UV-B radiation on antioxidant defense system in sunflower cotyledons. Plant Science 162, 939-
- Dizengremel P., Vaultier M.-N., Le Thiec D., Cabané M., Bagard M., Gérant D. & Jolivet Y. (2012) Phosphoenolpyruvate is at the crossroads of leaf metabolic responses to ozone stress. The New Phytologist 195, 512-517.
- Dubos C., Stracke R., Grotewold E., Weisshaar B., Martin C. & Lepiniec L. (2010) MYB transcription factors in Arabidopsis. Trends in Plant Science 15,
- Forcisi S., Moritz F., Kanawati B., Tziotis D., Lehmann R. & Schmitt-Kopplin P. (2013) Liquid chromatography-mass spectrometry in metabolomics research: mass analyzers in ultra high pressure liquid chromatography coupling. Journal of Chromatography. A 1292, 51-65.

- Ghirardo A., Gutknecht J., Zimmer I., Brueggemann N. & Schnitzler J.-P. (2011) Biogenic volatile organic compound and respiratory CO2 emissions after C-13-labeling: online tracing of C translocation dynamics in poplar plants. PLoS ONE 6, e17393.
- Ghirardo A., Heller W., Fladung M., Schnitzler J.P. & Schroeder H. (2012) Function of defensive volatiles in pedunculate oak (Quercus robur) is tricked by the moth Tortrix viridana. Plant, Cell & Environment 35, 2192-2207.
- Gil M., Pontin M., Berli F., Bottini R. & Piccoli P. (2012) Metabolism of terpenes in the response of grape (Vitis vinifera L.) leaf tissues to UV-B radiation. Phytochemistry 77, 89-98.
- Gonzalez A., Zhao M., Leavitt J.M. & Lloyd A.M. (2008) Regulation of the anthocyanin biosynthetic pathway by the TTG1/bHLH/Myb transcriptional complex in Arabidopsis seedlings. The Plant Journal 53, 814-827.
- Green A.E.S., Sawada T. & Shettle E.P. (1974) The middle ultraviolet reaching the ground. Photochemistry and Photobiology 19, 251-259.
- Haldimann P., Fracheboud Y. & Stamp P. (1995) Carotenoid composition in Zea mays developed at sub-optimal temperature and different light intensities. Physiologia Plantarum 95, 409-414.
- Hansel A., Jordan A., Holzinger R., Prazeller P., Vogel W. & Lindinger W. (1995) Proton transfer reaction mass spectrometry; on-line trace gas analysis at the ppb level. International Journal of Mass Spectrometry and Ion Processes 149-150, 609-619.
- Hanson D.T. & Sharkey T.D. (2001) Rate of acclimation of the capacity for isoprene emission in response to light and temperature. Plant, Cell & Environment, 24, 937-946.
- Harborne J.B. & Williams C.A. (2000) Advances in flavonoid research since 1992. Phytochemistry 55, 481-504.
- Harley P., Deem G., Flint S. & Caldwell M. (1996) Effects of growth under elevated UV-B on photosynthesis and isoprene emission in Quercus gambelii and Mucuna pruriens. Global Change Biology 2, 149-154.
- Heijde M. & Ulm R. (2012) UV-B photoreceptor-mediated signalling in plants. Trends in Plant Science 17, 230-237.
- Heine G.F., Hernandez J.M. & Grotewold E. (2004) Two cysteines in plant R2R3 MYB domains participate in REDOX-dependent DNA binding. The Journal of Biological Chemistry 279, 37878-37885.
- Hideg E., Jansen M. & Strid A. (2013) UV-B exposure, ROS, and stress: inseparable companions or loosely linked associates? Trends in Plant Science 18, 107–115.
- Hoch W.A., Singsaas E.L. & McCown B.H. (2003) Resorption protection. Anthocyanins facilitate nutrient recovery in autumn by shielding leaves from potentially damaging light levels. Plant Physiology 133, 1296–1305.
- Huang T., Tohge T., Lytovchenko A., Fernie A.R. & Jander G. (2010) Pleiotropic physiological consequences of feedback-insensitive phenylalanine biosynthesis in Arabidopsis thaliana. The Plant Journal 63, 823-835.
- Hutzler P., Fischbach R., Heller W., Jungblut T.P., Reuber S., Schmitz R. & Schnitzler J.P. (1998) Tissue localization of phenolic compounds in plants by confocal laser scanning microscopy. Journal of Experimental Botany 49,
- Ibrahim R.K., De Luca V., Khouri H., Latchinian L., Brisson L. & Charest P.M. (1987) Enzymology and compartmentation of polymethylated flavonol glucosides in chrysosplenium americanum. Phytochemistry 26, 1237–1245.
- Jansen M.A.K., Gaba V. & Greenberg B. (1998) Higher plants and UV-B radiation: balancing damage, repair and acclimation. Trends in Plant Science
- Jenkins G.I. (2009) Signal transduction in responses to UV-B radiation. Annual Review of Plant Biology 60, 407-431.
- Jiao Y., Lau O.S. & Deng X.W. (2007) Light-regulated transcriptional networks in higher plants. Nature Review Genetics 8, 217-230.
- Kaspar S., Matros A. & Mock H.P. (2010) Proteome and flavonoid analysis reveals distinct responses of epidermal tissue and whole leaves upon UV-B radiation of barley (Hordeum vulgare L.) seedlings. Journal of Proteome Research 9, 2402-2411.
- Kim S., Yun E., Hossain M.A., Lee H. & Kim K. (2012) Global profiling of ultraviolet-induced metabolic disruption in Melissa officinalis by using gas chromatography-mass spectrometry. Analytical and Bioanalytical Chemistry 404, 553-562.
- Koes R., Verweij W. & Quattrocchio F. (2005) Flavonoids: a colorful model for the regulation and evolution of biochemical pathways. Trends in Plant Science 10, 236-242.
- Kusano M., Tohge T., Fukushima A., Kobayashi M., Hayashi N., Otsuki H. & Fernie A.R. (2011) Metabolomics reveals comprehensive reprogramming

- involving two independent metabolic responses of Arabidopsis to UV-B light. The Plant Journal 67, 354-369.
- Lake J.A., Field K.J., Davey M.P., Beerling D.J. & Lomax B.H. (2009) Metabolomic and physiological responses reveal multi-phasic acclimation of Arabidopsis thaliana to chronic UV radiation. Plant, Cell & Environment 32,
- Landry L.G., Chapple C.C.S. & Last R.L. (1995) Arabidopsis mutants lacking phenolic sunscreens exhibit enhanced ultraviolet-B injury and oxidative damage. Plant Physiology 109, 1159-1166.
- Lau O.S. & Deng X.W. (2012) The photomorphogenic repressors COP1 and DET1: 20 years later. Trends in Plant Science 17, 584-593.
- Lavola A. (1998) Accumulation of flavonoids and related compounds in birch induced by UV-B irradiance. Tree Physiology 18, 53-58.
- Li J., Oulee T.M., Raba R., Amundson R.G. & Last R.L. (1993) Arabidopsis flavonoid mutants are hypersensitive to UV-B irradiation. The Plant Cell 5, 171_179
- Li Z. & Sharkey T.D. (2013) Metabolic profiling of the methylerythritol phosphate pathway reveals the source of post-illumination isoprene burst from leaves. Plant, Cell & Environment 36, 429-437.
- Lidon F.J.C., Teixeira M. & Ramalho J.C. (2012) Decay of the chloroplast pool of ascorbate switches on the oxidative burst in UV-B-irradiated rice. Journal of Agronomy and Crop Science 198, 130-144.
- Loreto F. & Schnitzler J.P. (2010) Abiotic stresses and induced BVOCs. Trends in Plant Science 15, 154-166.
- Lucio M., Fekete A., Frommberger M. & Schmitt-Kopplin P. (2011) Metabolomics: high-resolution tools offer to follow bacterial growth on a molecular level. In: Handbook of Molecular Microbial Ecology I, pp. 683-695. John Wiley & Sons, Inc.
- Maeda H. & Dudareva N. (2012) The shikimate pathway and aromatic amino acid biosynthesis in plants. Annual Review of Plant Biology 63, 73-105.
- Martens H. & Martens M. (2000) Modified Jack-knife estimation of parameter uncertainty in bilinear modelling by partial least squares regression (PLSR). Food Quality and Preference 11, 5-16.
- Monson R.K., Jones R.T., Rosenstiel T.N. & Schnitzler J.-P. (2013) Why only some plants emit isoprene. Plant, Cell & Environment 36, 503-516.
- Oikawa A., Nakamura Y., Ogura T., Kimura A., Suzuki H., Sakurai N., . . . Ohta D. (2006) Clarification of pathway-specific inhibition by fourier transform ion cyclotron resonance/mass spectrometry-based metabolic phenotyping studies. Plant Physiology, 142, 398-413.
- Pietta P.-G. (2000) Flavonoids as antioxidants. Journal of Natural Products 63, 1035-1042.
- Quideau S., Deffieux D., Douat-Casassus C. & Pouységu L. (2011) Plant polyphenols: chemical properties, biological activities, and synthesis. Angewandte Chemie International Edition 50, 586-621.
- Razal R.A., Ellis S., Singh S., Lewis N.G. & Towers G.H.N. (1996) Nitrogen recycling in phenylpropanoid metabolism. Phytochemistry 41,
- Riederer M. & Schreiber L. (2001) Protecting against water loss: analysis of the barrier properties of plant cuticles. Journal of Experimental Botany 52, 2023-2032.
- Ries G., Heller W., Puchta H., Sandermann H., Seidlitz H.K. & Hohn B. (2000) Elevated UV-B radiation reduces genome stability in plants. Nature 406,
- Rizzini L., Favory J.J., Cloix C., Faggionato D., O'Hara A., Kaiserli E. & Ulm R. (2011) Perception of UV-B by the Arabidopsis UVR8 protein. Science
- Schmelzer E., Jahnen W. & Hahlbrock K. (1988) In situ localization of lightinduced chalcone synthase mRNA, chalcone synthase, and flavonoid end products in epidermal cells of parsley leaves. Proceedings of the National Academy of Sciences 85, 2989-2993.
- Schnitzler J.P., Jungblut T.P., Heller W., Kofferlein M., Hutzler P., Heinzmann U. & Sandermann H. (1996) Tissue localization of UV-B-screening pigments and of chalcone synthase mRNA in needles of Scots pine seedlings. The New Phytologist 132, 247-258.
- Schnitzler J.P., Louis S., Behnke K. & Loivamaki M. (2010) Poplar volatiles biosynthesis, regulation and (eco)physiology of isoprene and stress-induced isoprenoids. Plant Biology 12, 302-316.
- Seckmeyer G., Pissulla D., Glandorf M., Henriques D., Johnsen B., Webb A. & Carvalho F. (2008) Variability of UV irradiance in Europe. Photochemistry and Photobiology 84, 172-179.
- Sharkey T. & Loreto F. (1993) Water stress, temperature, and light effects on the capacity for isoprene emission and photosynthesis of kudzu leaves. Oecologia 95, 328-333.

- Sharkey T.D. & Yeh S.S. (2001) Isoprene emission from plants. Annual Review of Plant Physiology and Plant Molecular Biology 52, 407-436.
- Shin D.H., Choi M., Kim K., Bang G., Cho M., Choi S.-B. & Park Y.-I. (2013) HY5 regulates anthocyanin biosynthesis by inducing the transcriptional activation of the MYB75/PAP1 transcription factor in Arabidopsis. FEBS Letters 587, 1543-1547.
- Shinbo Y., Nakamura Y., Altaf-Ul-Amin M., Asahi H., Kurokawa K., Arita M., . . . Kanaya S. (2006) KNApSAcK: a comprehensive species-metabolite relationship database. In: Plant Metabolomics (eds K. Saito, R. Dixon, & L. Willmitzer), pp. 165-181. Springer Berlin Heidelberg.
- Sims D.A. & Gamon J.A. (2002) Relationships between leaf pigment content and spectral reflectance across a wide range of species, leaf structures and developmental stages. Remote Sensing of Environment 81, 337-354.
- Smith C., O'Maille G., Want E., Qin C., Trauger S., Brandon T., . . . Siuzdak G. (2005) METLIN - A metabolite mass spectral database. Therapeutic Drug Monitoring, 27, 747–751.
- Strid A., Chow W.S. & Anderson J.M. (1994) UV-B damage and protection at the molecular level in plants. Photosynthesis Research 39, 475-489.
- Suhre K. & Schmitt-Kopplin P. (2008) MassTRIX: mass translator into pathways. Nucleic Acids Research, 36, 481-484.
- Tanaka Y., Sasaki N. & Ohmiya A. (2008) Biosynthesis of plant pigments: anthocyanins, betalains and carotenoids. The Plant Journal 54, 733-749.
- Thayer S. & Björkman O. (1990) Leaf xanthophyll content and composition in sun and shade determined by HPLC. Photosynthesis Research 23, 331-343.
- Thiel S., Döhring T., Köfferlein M., Kosak A., Martin P. & Seidlitz H. (1996) A phytotron for plant stress research: how far can artificial lighting compare to natural sunlight? Journal of Plant Physiology 148, 456-463.
- Tiiva P., Rinnan R., Faubert P., Räsänen J., Holopainen T., Kyrö E. & Holopainen J.K. (2007) Isoprene emission from a subarctic peatland under enhanced UV-B radiation. The New Phytologist 176, 346-355.
- Tossi V., Amenta M., Lamattina L. & Cassia R. (2011) Nitric oxide enhances plant ultraviolet-B protection up-regulating gene expression of the phenylpropanoid biosynthetic pathway. Plant, Cell & Environment 34, 909-
- Vanderauwera S., Zimmermann P., Rombauts S., Vandenabeele S., Langebartels C., Gruissem W. & Van Breusegem F. (2005) Genome-wide analysis of hydrogen peroxide-regulated gene expression in Arabidopsis reveals a high light-induced transcriptional cluster involved in anthocyanin biosynthesis. Plant Physiology 139, 806-821.
- Warren J., Bassman J., Fellman J., Mattinson D. & Eigenbrode S. (2003) Ultraviolet-B radiation alters phenoloc salicylate and flavonoid composition of Populus trichocarpa leaves. Tree Physiology 23, 527-535.
- Way D.A., Ghirardo A., Kanawati B., Esperschütz J., Monson R.K., Jackson R.B. & Schnitzler J.-P. (2013) Increasing atmospheric CO2 reduces metabolic and physiological differences between isoprene- and non-isoprene-emitting poplars. The New Phytologist 200, 534-546.
- Winkel-Shirley B. (2001) Flavonoid biosynthesis. A colorful model for genetics, biochemistry, cell biology, and biotechnology. Plant Physiology 126, 485-493.
- Woodall G.S. & Stewart G.R. (1998) Do anthocyanins play a role in UV protection of the red juvenile leaves of Syzygium? Journal of Experimental Botany 49, 1447-1450.
- Yamasaki H., Sakihama Y. & Ikehara N. (1997) Flavonoid-peroxidase reaction as a detoxification mechanism of plant cells against H2O2. Plant Physiology
- Zhang P., Dreher K., Karthikeyan A., Chi A., Pujar A., Caspi R., . . . Rhee S.Y. (2010) Creation of a genome-wide metabolic pathway database for populus trichocarpa using a new approach for reconstruction and curation of metabolic pathways for plants. Plant Physiology, 153, 1479-1491.
- Zhou B., Miao Q., Yang L. & Liu Z.-L. (2005) Antioxidative effects of flavonols and their glycosides against the free-radical-induced peroxidation of linoleic acid in solution and in micelles. Chemistry - A European Journal 11, 680-691.
- Zhou J.-M., Gold N.D., Martin V.J.J., Wollenweber E. & Ibrahim R.K. (2006) Sequential O-methylation of tricetin by a single gene product in wheat. Biochimica et Biophysica Acta (BBA) – General Subjects 1760, 1115–1124.

Received 22 October 2013; received in revised form 26 March 2014; accepted for publication 27 March 2014

SUPPORTING INFORMATION

Additional Supporting Information may be found in the online version of this article at the publisher's web-site:

Figure S1. Growing conditions of (a) air temperature, relative air humidity, PAR and UV-B radiation during the 16/8 h day/night cycle in the sun simulators including daily doses of PAR and UV-B radiation [UVB: energetically weighted UV-B radiation, UV-B_{Be}: biologically effective UV-B radiation after Green et al. (1974) according to measurements of Caldwell (1971) normalized at 300 nm]. Irradiation conditions of (b) PAR, UV-A, UV-B and biologically effective UV-B radiation in the control and treatment chambers during the acclimation and experiment.

Figure S2. Picture of the experimental set-up in a treatment chamber.

Figure S3. Time course of photosynthetic pigments. Ratio of xanthophyll/chlorophyll a ratio in (a) IE poplar and (b) in NE poplar leaves. Ratio of carotenoid/chlorophyll a in (c) IE and (d) in NE poplar leaves. Zeaxanthin and Antheraxanthin content in (e) IE and (f) in NE poplar leaves. Bars in the figure indicate least significant difference values (ANOVA, Fisher's LSD test). WT/UV-, →; EV/UV-, →; WT/UV+, →; EV/UV+, →; Ra2/UV-, →; Rb7/UV-, →; Ra2/UV+, **--**; Rb7/UV+, **-**-.

Figure S4. Time course of standard isoprene emission and net CO₂ assimilation rates. Net CO₂ assimilation rates in (a) IE and (b) in NE poplar leaves. Isoprene emission rates in of (c) IE and (d) NE poplar lines. Evaporation rates of (e) IE and (f) NE poplar lines. Standard conditions (leaf temperature: 30 °C, PAR: 1000 μmol photons m⁻² s⁻¹) Bars in the figure indicate least significant difference values (ANOVA, Fisher's LSD test). WT/UV-, -; EV/UV-, -; WT/UV+, -; EV/UV+, -0-; Ra2/UV−, -1-; Rb7/UV−, -1-; Ra2/UV+, -1-; $Rb7/UV+, -\Gamma$.

Figure S5. Time course of stomatal conductance of (a) IE and (b) NE poplars at control and UV-B conditions. WT/UV-, →; EV/UV-, -○-; WT/UV+, →; EV/UV+, -○-; Ra2/UV-, --; Rb7/UV-, -□-; Ra2/UV+, --; Rb7/UV+, -□-.

Figure S6. Pathway overview of annotated metabolites that were discriminant for the separation of NE from IE poplar leaves. Annotations were sorted according to the KEGG categorization.

Figure S7. Pathway overview of annotated metabolites that were discriminant for the UV treatment. Annotations were sorted according to the KEGG categorization.

Table S1. Complete list of annotated discriminant masses with database ID, number of isomers, pathway name and Kegg map ID. Annotations with no Kegg map ID are not found in Kegg maps. List does not include annotated isotope masses (80 annotations).